Photoacoustic measurement of methane concentrations with a compact pulsed optical parametric oscillator

András Miklós, Chin-How Lim, Wei-Wei Hsiang, Geng-Chiau Liang, A. H. Kung, Andreas Schmohl, and Peter Hess

A pulsed periodically poled lithium niobate optical parametric oscillator operating in a cavity with a grazing-incidence grating configuration was used for sensitive and precise measurement of trace quantities of methane in nitrogen by photoacoustic spectroscopy with a novel differential photoacoustic detector. A sensitivity of 1.2 parts in 10^9 by volume of methane was obtained in direct calibration measurements (not extrapolated). With this apparatus, *in situ* measurement of the methane concentration in ambient air under atmospheric conditions was demonstrated. © 2002 Optical Society of America

OCIS codes: 300.6430, 300.6360, 190.4970.

1. Introduction

Recent improvements in compact all-solid-state tunable lasers, such as tunable diode lasers, quantum-cascade lasers, and optical parametric oscillators, radiating in the mid-infrared spectral region have significantly advanced the application of lasers in trace-gas monitoring. The optical techniques commonly used in trace-gas detection are absorption spectroscopy,[1–6] cavity ringdown spectroscopy,[7,8] and photoacoustic spectroscopy.[9–13] Usually the lasers are operated in the continuous-wave single-frequency mode. The advantages of using these high-resolution continuous-wave lasers are their excellent selectivity and high sensitivity, and the potential for rapid wavelength scanning. However, one or more of the following shortcomings have hindered the broad practical utilization of these lasers: low power, complex operation, limited continuous scanning range, and the need for stringent electronic and temperature control to maintain wavelength stability.

Sensitive photoacoustic (PA) detection of methane was introduced in 1971 in a pioneering paper by Kreuzer, who used the accidental coincidence between the 3.39-μm emission of the He–Ne laser and an absorption line of the asymmetric stretching vibration of methane.[9] Experimental data were presented to approximately 1 part in 10^6 by volume (ppmv), and it was stated that a sensitivity of 100 parts in 10^9 by volume (ppbv) was achieved with a 15-mW He–Ne laser. In subsequent development of PA trace-gas detection, chiefly CO_2 and CO lasers were used because of their higher power and line tunability. Methane could not be excited with these lasers. Hence near-infrared diode lasers,[14] optical parametric oscillators, and difference-frequency mixing[15–17] were employed to detect methane (however, with limited sensitivity).

Recently a periodically poled lithium niobate (PPLN) optical parametric oscillator that uses a simple grazing-incidence grating cavity configuration (GIOPO) for broad and fast wavelength tuning was developed for the mid-infrared region. This GIOPO is capable of producing several tens to one hundred milliwatts of infrared power in a bandwidth of 0.2 cm^{-1} in the 1–2-μm region (signal beam) and of 0.8 cm^{-1} in the 3-μm region (idler beam).[18] In a typical atmospheric condition the pressure-broadened linewidth of most gases is in the range of a few tenths of a wave number. Thus, in open field applications the

A. Miklós, A. Schmohl, and P. Hess are with the Institute of Physical Chemistry, University of Heidelberg, Im Neuenheimer Feld 253, D-69120, Heidelberg, Germany. C.-H. Lim, W.-W. Hsiang, G.-C. Liang, and A. H. Kung (akung@po.iams.sinica.edu.tw) are with the Institute of Atomic and Molecular Sciences, Academia Sinica, P.O. Box 23-166, Taipei 106, Taiwan.

Received 3 August 2001; revised manuscript received 20 December 2001.

0003-6935/02/152985-09$15.00/0

© 2002 Optical Society of America

pressure-broadened linewidth of the detected species (several gigahertz) reduces the significance of the ultranarrow-linewidth attribute of single-mode lasers, making the cost and the complex operation associated with a narrow linewidth more a liability than an asset. Instead, a GIOPO idler output with a bandwidth of 0.2–0.3 cm^{-1} is more suitable for exciting the species.

When it is pumped by a laser-diode pumped *Q*-switched Nd:YAG laser the GIOPO runs at a repetition rate of several kilohertz, matching the lowest acoustic resonance of a resonant photoacoustic cell designed for sensitive spectroscopy and gas analysis.[10] In a previous experiment the signal output of the GIOPO was used in combination with a single resonator PA cell to excite methane in the first vibrational overtone in the near infrared, resulting in a detection sensitivity of 20–30 ppbv.[19] For practical applications, however, it is essential to realize higher sensitivities, which are achievable by exciting fundamental vibrational modes, and to be able to operate in an ambient flow environment.

Another sensitive method of methane detection is tunable infrared-laser differential absorption spectroscopy. In the infrared such measurements are performed with lead-salt diode lasers cooled to liquid-nitrogen temperature.[1,2] Recent advances in multipass cell configurations have significantly extended the sensitivity of the absorption technique. Using a White or a Herriott cell with a path length of approximately 100 m can drastically increase the absorption. For example, with four diode lasers (3.4–8 μm) and HgCdTe detectors in a single liquid-nitrogen Dewar and a 1-m long, 80-pass Herriott cell, simultaneous measurements of HCl, NO_2, N_2O, HNO_3, and CH_4 were made with sensitivities that reached the sub-ppbv range.[1] The disadvantages of this method are the necessity to cool the laser and detector and the relatively large size and volume of the gas cell.

The importance of atmospheric methane is well established. In recent years several studies have identified the critical role of methane in global warming and determined its chemistry in the troposphere and the stratosphere.[20] Besides the well-known sources of methane, such as chemical facilities, industrial plants, and mines, other methane sources are now being studied carefully. For example, rice paddies are a major contributor to the global methane budget.[21] Also, sources of greenhouse gas that have climatic relevance in the future are of interest. Isotopic signals have been identified that provide evidence of a massive release of methane 180 million years ago.[22] In the past, greenhouse warming may have caused a sudden release of methane from the gas hydrates (water and methane) in ocean sediments, as recorded in a negative carbon-isotope anomaly.

To control the global increase in atmospheric methane it is prudent to monitor the spatial distribution of methane in the atmosphere and to quantify the magnitude of various emission sources.[23] Spectroscopic methods facilitate precise *in situ* data acquisition.

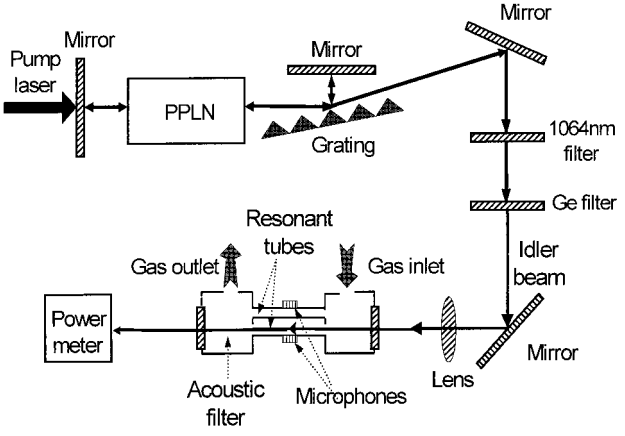

Fig. 1. Experimental setup with pump laser, GIOPO, and photoacoustic detector.

Under atmospheric conditions, two factors have a major influence on the spectroscopic detection of methane. The first is pressure broadening of the spectral lines to a few tenths to several tenths of a wave number. The second factor is the presence of other species in air, especially water vapor, whose concentration is a few percent at standard temperature and pressure. Near 3000 cm^{-1}, water has an abundance of absorption lines that overlap most of the methane lines. A high concentration of water vapor requires high selectivity, and thus spectroscopic methods are needed to detect trace amounts of gases in ambient air. According to a careful study of the methane spectrum in this region by use of the HITRAN database, the methane line at 2948 cm^{-1} is essentially free of interference from water.[24] Therefore we have chosen the spectral region near this line with which to demonstrate the usefulness of the GIOPO for precise and sensitive methane detection in air.

In this paper we report the results of operating the GIOPO in the idler mode to excite a fundamental vibrational mode of methane and using a dual-resonator cell to achieve higher sensitivities. We applied the carefully calibrated system to measure the concentration of methane in ambient air. Here we show that a 0.8-cm^{-1} GIOPO is sufficient to demonstrate the measurement sensitivity of the GIOPO in a single-gas experiment. For applications in multicomponent analysis in which high selectivity is desired, a reduction of the GIOPO idler bandwidth to 0.2 cm^{-1} will be required.

2. Experimental Setup

The experimental setup shown in Fig. 1 is similar to that applied previously[19]; it includes a GIOPO and a photoacoustic detection system. The GIOPO was operated with a PPLN crystal period of 29.7 μm. The crystal was placed in an oven whose temperature could be varied from room temperature to 210 °C with a temperature stability of ±0.2 °C. A 1064-nm filter and an antireflection-coated Ge filter were used to block the residual pump-laser light and the signal

beam from the GIOPO and to pass the idler output to the PA cell. Continuous fine scanning of the idler wavelength was carried out with a micro stepping motor controlled by a PC. The scan speed was 1 s/step, with a step size of 0.03 cm^{-1}. We could cover a distance of ~20 cm^{-1} without changing the crystal temperature. It typically took ~5 min to complete such a scan. After the Ge filter the average output power was typically 60 mW. Two gold-coated copper mirrors (radius of curvature, 50 cm) were used to focus the infrared beam into one of the two identical resonator tubes (inner diameter, 5.5 mm) of a differential PA detector.

The PA detector employed was designed for fast time response (~10 s), low electronic and acoustic noise, and high sensitivity. The device had a fully symmetrical design, with dual acoustic resonator tubes sandwiched between two acoustic filters. A microphone (Knowles 3029) was placed in the central section of each tube flush with the wall. The gas mixture flowed continuously through both resonator tubes, but the laser beam was passed through only one resonator. Both microphone signals were amplified by a differential amplifier to reduce the flow noise substantially. The repetition rate of the pump laser at 1064 nm was adjusted to match the longitudinal acoustic resonance frequency of the tube at 4100 Hz. The Q factor of the resonator was $Q = 17$, which corresponds to a FWHM for the resonance of ~235 Hz for nitrogen at room temperature. Because the repetition rate could be adjusted only in 10-Hz steps, perfect matching was not possible. The error in the PA signal that was caused by this frequency mismatch, however, was smaller than 1%. A gas flow rate of 300 standard cubic centimeters per minute at STP (SSCM) was used throughout all the experiments. Because the volume of the acoustic filter between the gas inlet and two resonator tubes was ~17 cm^3 and that of the resonator tubes was ~2 cm^3, a time delay of 3.4 s and a rise time of 0.4 s could be calculated for the PA signal from the nominal gas flow rate. Thus a response time of ~4 s could be expected for sudden concentration changes that occurred at the input of the PA detector. The measured response time of a similar PA detector[25] was somewhat longer, namely, ~10 s.

The photoacoustic signal was measured with a phase-sensitive lock-in amplifier (SRS Model 835) and recorded with a PC. We plotted the PA signal, normalized to the power of the infrared output from the GIOPO, as a function of the idler wavelength to obtain the PA spectrum.

3. Results

A. Calibration Measurements and Data Analysis

The sensitivity of the GIOPO PA system for measuring methane concentrations with idler radiation was determined by calibration measurements. A certified mixture of 0.900-ppmv of methane in nitrogen was employed. The absorption spectrum of the asymmetric stretching vibration of methane was measured by subsequent scans (~20 cm^{-1}) of the GIOPO with stepwise increased temperature. We scanned the wavelength of the GIOPO over a total range of 200 cm^{-1}, using a scan step size of 0.03 cm^{-1} and a 1-s time constant for averaging the lock-in amplifier signal. The temperature step size was 2 °C. The temperature range covered was 115–210 °C. The total scan time was ~6 h. Much of the 6 h was taken by the oven to reach a stabilized temperature at each temperature step. This scan time could have been significantly shorter if the crystal temperature had been computer synchronized to the wavelength. The corresponding power normalized photoacoustic spectrum is shown in Fig. 2. Also displayed for comparison is the spectrum generated from HITRAN for 0.900-ppmv of methane in nitrogen at 760 Torr and 25 °C, convoluted with a Gaussian laser profile of 0.8-cm^{-1} width. As can be seen, the agreement between the two is reasonably good. Some discrepancies occur in the wavelength scale as the result of a small calibration error of the GIOPO scan, and in the amplitude because of normalization errors of the PA signal at low GIOPO powers.

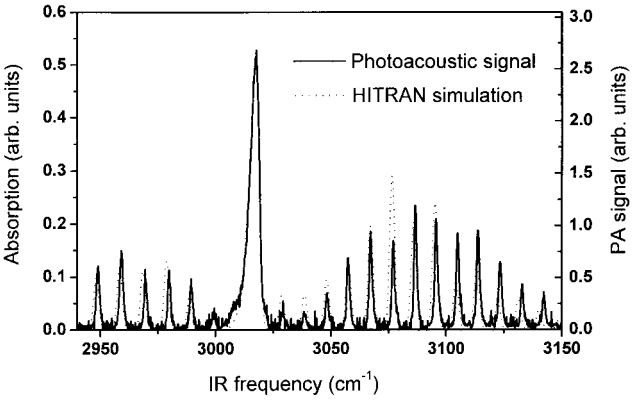

Fig. 2. Comparison of the normalized photoacoustic methane spectrum of the asymmetric stretching vibration with the spectrum simulated by use of the HITRAN data base.

For the calibration measurements the GIOPO was tuned to the peak of the Q branch to produce the highest sensitivity. We optimized the GIOPO power by adjusting both the grating and the PPLN crystal's temperature. We diluted the mixture of 900 ppbv of methane in nitrogen by mixing it with a dry-nitrogen gas flow. The nitrogen gas was derived from the boil-off of a liquid-nitrogen storage tank. Its purity was at least 99.999%, with an undetectable amount of water. The quantity of gas flow of each gas was set by high-resolution mass-flow controllers (MFCs; Brooks 5850E series).

The volume flow of nitrogen was controlled by a MFC that had a full range of 1000 sccm, three MFCs (full ranges 300, 80, and 20 sccm) were used for controlling the flow of the certified mixture. The MFCs were adjusted to maintain a total volume flow of 300 sccm. Three different calibration measurements were carried out. The concentration of methane was reduced from 900 to 18 ppbv in 22 steps (by MFC

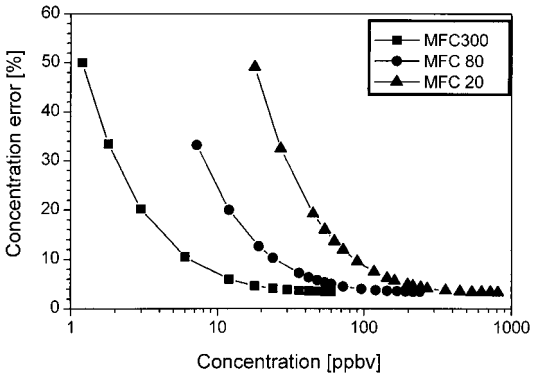

Fig. 3. Relative concentration errors of the three calibration measurements as a function of methane concentration.

300), from 240 to 7.2 ppbv in 17 steps (by MFC 80), and from 60 to 1.2 ppbv in 13 steps (by MFC 20). The error of the concentration was determined from the errors of the MFCs (1% of the full range).

The relative error of the concentration is shown in Fig. 3. Because the absolute error of the MFCs is constant, the relative error increases drastically for low-flow settings of the MFCs. Therefore the error of the concentration approaches 50% at the lowest concentrations of the three curves.

The magnitude and the phase of the photoacoustic signal were measured by the lock-in amplifier. The background signal was detected in a pure-nitrogen flow, whereas we determined the noise (flow, acoustic, and electromagnetic noise) by blocking the laser beam. The magnitude and the phase of the PA signal and the magnitude of the light power were read and stored by use of a Labview program. Approximately 60 PA magnitude and phase values were collected at each concentration. The average and the standard deviation (σ) of these data were used as experimental result and error, respectively, for the corresponding concentration. All relative errors (standard deviation/average) were smaller than 1.6%. The measured amplitudes from the lock-in amplifier were normalized to 40-mW light power (the average power during the three experiments) to produce comparable values. The standard deviations of the light-power data were below 0.2 mW ($\sim$0.5%).

First the noise performance was checked with gas flow. The intrinsic noise of the miniature electret microphones was very large; an approximate value of 15–20 μV was measured for the broadband noise. However, this noise was completely uncorrelated. The noise measured by the lock-in amplifier (time constant, 1 s) when the laser beam was blocked was 0.34 μV. The background signal that was due to the laser measured with pure nitrogen was approximately eleven times larger (3.80 μV).

Because the background is usually coherent with the exciting laser light, i.e., it has a quite stable phase lag of Θ_{BG} to the lock-in reference, and the PA signal has another constant phase Θ_{PA}, the measured signal U_{PA} can be regarded as the vectorial sum of constant background B, signal S, and incoherent noise N in the form

$$U_{PA} = [S^2 + 2SB\cos(\theta_{PA} - \theta_{BG}) + B^2 + N^2]^{1/2}. \quad (1)$$

Taking into account that PA signal S is strictly linear with concentration x,[26,27] we can use the following function to fit the measured PA signal:

$$U_{PA} = [(ax)^2 + bx + c^2]^{1/2}, \quad (2)$$

where U_{PA} and x are the measured PA signal [μV] and the concentration in ppbv, respectively. Fit parameter a is the sensitivity of the PA methane detector [μV/ppbv]. The meaning of fit parameters b and c can be seen from comparison of Eqs. (1) and (2).

Because the function of Eq. (2) could be fitted quite well to the data of the three calibration experiments, the measurements confirm the assumption introduced above: The measured PA signal can in fact be regarded as a vectorial sum of a linear PA signal and a coherent background. The fit parameters and their errors are summarized in Table 1. The residuals (the deviation of the measured values from the fit curve) were smaller than 1% for all three measurements. However, the differences between the corresponding fit parameters determined from the various measurements were in some cases significant; i.e. the confidence intervals ($\pm 3\sigma$ ranges) do not overlap.

It was assumed that these deviations of the parameter values are caused mainly by the large errors connected with the concentrations. Therefore the best values (PA data with the smallest concentration errors) were selected from the three calibration measurements, and a vectorial fit was made. The measured PA data points, the curve fitted with Eq. (2), and the truly linear PA signal given by the product ax are shown in Fig. 4. The fit parameters a, b, and c and their errors are presented in the bottom row of Table 1.

The calculated curve presented in Fig. 4 fits the measured PA data points well. The residuals of the fit and the $\pm 1\sigma$ curves are shown in Fig. 5. As can be seen, the data points were selected from three differ-

Table 1. Parameters of the Vectorial Fit to the Experimental Data

Concentration (ppbv)	a (μV/ppbv)	Δa (μV/ppbv)	b (μV^2/ppbv)	Δb (μV^2/ppbv)	c (μV)	Δc (μV)
900–18	0.09176	0.00027	0.698	0.029	3.922	0.239
240–7.2	0.09208	0.00082	0.473	0.029	3.815	0.105
60–1.2	0.090	0.022	0.470	0.022	3.847	0.0023
900–1.2	0.09365	0.00028	0.454	0.026	3.823	0.123

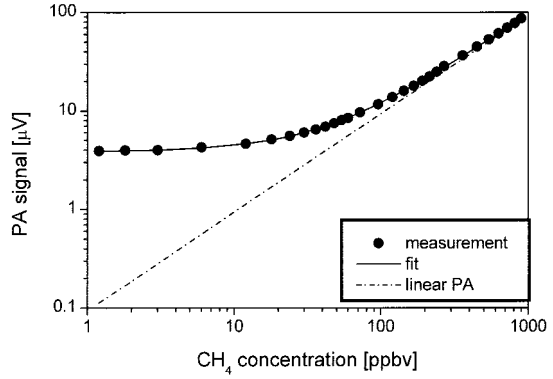

Fig. 4. Comparison of measured PA signals, the curve fitted with Eq. (2), and the true linear PA signal given by the product αx.

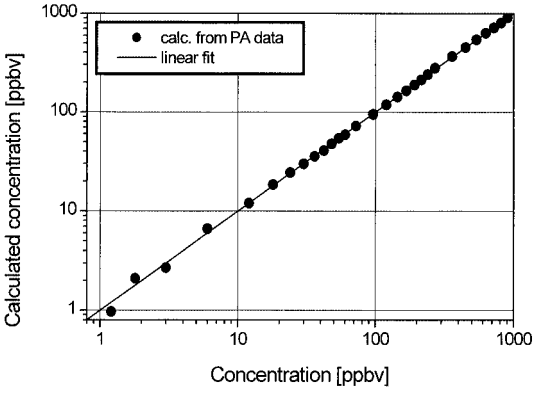

Fig. 6. Comparison of the calculated concentration with those adjusted by the MFCs.

ent measurements because the residuals exhibit characteristic differences in the three concentration domains. Nevertheless, the deviation from the fit does not exceed 3% through the full concentration range, and the residuals are always inside the $\pm 1\sigma$ error curves. For this reason the fit curve can be regarded as the calibration curve of the photoacoustic methane detector at the selected wavelength. The photoacoustic sensitivity of the system is given by fit parameter a written in the last row of Table 1:

$$a = 0.09365 \pm 0.00028\ \mu\text{V/ppbv} \approx 0.09365\ \mu\text{V/ppbv} \pm 0.3\%. \quad (3)$$

As indicated in Fig. 4, the smallest measured methane concentration value was 1.2 ppbv with this setup. This directly measured low concentration (not extrapolated) is an improvement of more than 3 orders of magnitude over our previously reported result for which we had used the first overtone and is comparable with results extrapolated from measurements for which lasers or more-complicated detection schemes were used.[9,14]

The limiting sensitivity of the GIOPO PA detector for methane can be estimated from the standard deviations of the data points in Fig. 4. The average standard deviation (expressed in concentration) was 1.1 ppbv. This value can be regarded as the precision of the measurements and also as the limiting sensitivity with a signal-to-noise ratio of 1. The corresponding minimum detectable absorption coefficient is $\sim\alpha_{\min} \approx 3.3 \times 10^{-8}\ \text{cm}^{-1}$; the optical density, $\alpha_{\min} l \approx 1.3 \times 10^{-7}$. These numbers illustrate the high performance of the GIOPO PA detector for methane compared with that of optical absorption devices. Because the PA signal is proportional to the absorbed light power, it is better to characterize the sensitivity of the GIOPO PA detector by the following expression: $\alpha_{\min} P \approx 1.4 \times 10^{-9}\ \text{cm}^{-1}$ W, where P [W] is the power of the idler beam.

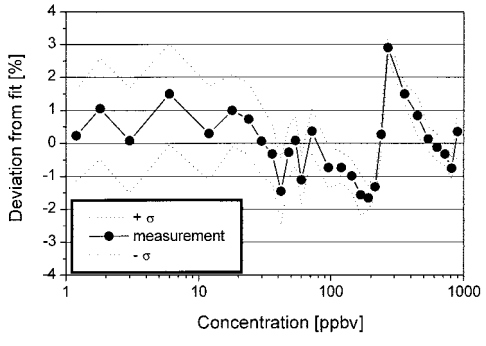

Fig. 5. Residuals of the fit of Fig. 4 and the $\pm 1\sigma$ curves.

B. Determination of Concentration from PA Measurements

The goal of photoacoustic trace-gas measurements is determination of the trace-gas concentration from the measured PA signal. One can carry out this procedure by calculating the concentration from the measured PA signal, using the fit parameters. The concentration can be expressed from Eq. (2) as

$$x = \frac{(U_{\text{PA}}{}^2 - c^2 + d^2)^{1/2} - d}{a}, \quad (4)$$

where

$$d = \frac{b}{2a} = \sqrt{c^2 - N^2}\cos(\theta_{\text{PA}} - \theta_{\text{BG}}). \quad (5)$$

The calculated concentration is plotted versus the selected concentration, determined from the mixing procedure, in Fig. 6. The calculated values are plotted as filled circles; the solid line shows the linear fit. The correlation coefficient is $R = 0.9994$, with a slope of the line of 0.99999, very close to the expected value of unity. The deviations of the calculated concentration values from the fitted line can be seen more clearly in Fig. 7. The deviations increase with decreasing concentration, as expected, but they do not exceed 20% even at the smallest concentration of 1.2 ppbv. That is, the error of the concentration values determined by means of the vectorial fit is smaller than the standard deviation of the measured data points.

Note that the concentrations calculated by Eq. (4) are highly sensitive to the value of parameter c,

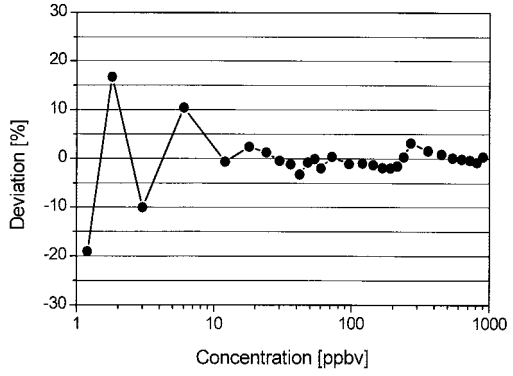

Fig. 7. Deviations of the calculated concentrations from the fitted curve.

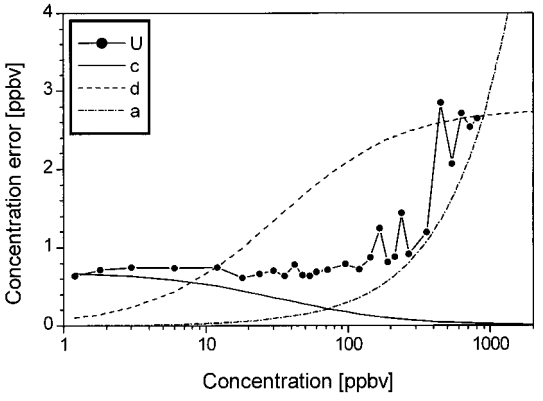

Fig. 8. Comparison of the experimental error with the contributions introduced by parameters a, c, and d.

which is the mean-square average of background B and noise N [cf. Eqs. (1) and (2)]. Therefore the accuracy of the concentration measurements in the low-concentration range, where the background is larger than the true PA signal, depends strongly on the stability of the background.

We determined the background at the end of the third calibration measurement by adjusting the methane concentration to zero (pure-nitrogen flow) and collecting 60 data points. The average value and the standard deviation of the background data points were determined as $B_{\mathrm{meas}} = (3.80 \pm 0.054)\ \mu\mathrm{V}$. This value is close to that of parameter c obtained from the calibration measurements (see the sixth column of Table 1). The standard deviation of B_{meas} was ~20 times smaller than the true linear PA signal at 1.2 ppbv (see the curve labeled linear PA in Fig. 4); thus the stability of the background was sufficient. However, different background values were found in the different calibration measurements. As it can be assumed that the background depends on the optical alignment (owing to the changes of light scattering and window reflection inside the PA cell), the optimization of the optical parametric oscillator preceding each measurement might lead to different background values. Because this problem is quite important for practical applications of the GIOPO PA system in trace-gas detection, a detailed investigation of the dependence of the background on the beam geometry and alignment is an important issue for future improvements of the technique.

The linear dependence of the PA signal on the concentration and the known behavior of both background and the noise facilitates calibration of the PA detector. In principle, it is sufficient to determine the sensitivity of the detector by measuring the PA signal (amplitude and phase) of three certified gas mixtures. One can then calculate three slope values by drawing a straight line through the origin and the calibration points. The average of the three slopes can be regarded as parameter a. This calibration method provides better results than a slope of the straight line fitted to the three calibration points, because in this case the slope is determined predominantly by the gas mixture with the highest concentration.

One can determine the amplitude and the phase of the background by measuring the PA signal in pure nitrogen and extract the noise by blocking the laser light. The amplitude of the measured background is given by parameter c. According to Eq. (1) the noise always contributes to the measured background. However, noise N is random; therefore it does not influence the phase of the background. Thus the value of parameter d can be calculated with Eq. (5).

Consequently, all parameters of Eq. (4) can be obtained by independent measurements. Concentration x can then be determined from the measured PA signal U_{PA} by use of Eq. (4). The accuracy of the concentration may also be derived from Eq. (4). Four main factors influence the error of the concentration: the error of the PA signal, the error of parameter c (the background), the error of parameter d, which contains also the errors of the phase values, and the error of PA sensitivity a. The contributions of these four factors are compared in Fig. 8. It can be seen that at low concentrations the errors of the background and the PA signal are dominant, whereas the error of parameter a determines the accuracy of the concentration measurements in the high-concentration range.

C. Measurements of Methane Concentration in Ambient Air

To demonstrate methane detection in ambient air, we sampled air from open space outside our laboratory with a dry pump and flowed it continuously through the PA cell. The flow rate was again set to 300 sccm by a calibrated MFC. A trap with an ice–rock salt mixture at -8 °C was used to reduce the water-vapor content of the air. The trap reduced the PA signal intensity of the water-vapor absorption lines in the spectrum at ~2950 cm^{-1} to a level comparable with the signal intensity of the methane lines to facilitate the display of the PA spectrum. Test measurements with the calibrated methane mixture proved that the concentration integrity of trace amounts of methane was not affected by the trap. It should be noted that in other analytical methods of trace-methane analy-

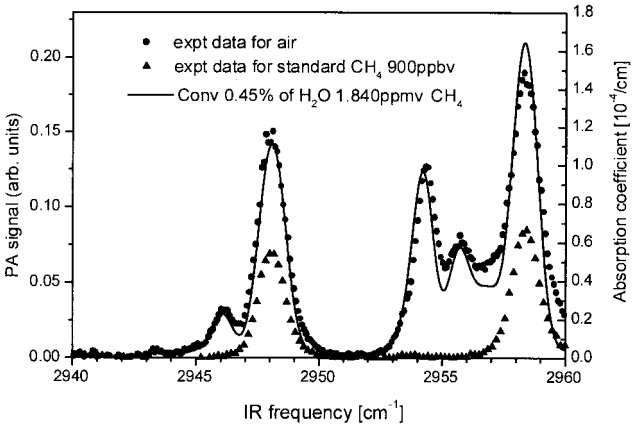

Fig. 9. Methane spectra measured for ambient air and the calibration sample with 900-ppbv methane compared with spectra simulated for a mixture of 0.45% water and 1840-ppbv methane.

sis, such as in gas chromatography, it is an accepted practice first to eliminate the water-vapor content in ambient air mixtures before the analysis.[20] For the measurement of the methane concentration in ambient air an absorption peak at 2948 cm^{-1} was selected because no water interference was found by HITRAN modeling at this peak. As can be seen from Fig. 2, approximately four times greater sensitivity was available by use of the peak of the *Q* branch. However, this measurement could not be performed at the *Q* branch because of large interference by water absorption.

The spectrum obtained for the air sample is presented in Fig. 9. The figure shows two methane peaks, at 2948 and at 2958 cm^{-1}. Other spectral features arise from the moisture that is still present in the air. A closer examination of the methane absorption spectrum and the water-vapor spectrum confirmed that, whereas most methane lines suffer from contamination by the more abundant water absorption, the intensity of the methane peak at 2948 cm^{-1} is not affected by any reasonable amount of water vapor. The methane concentration therefore can be determined directly from the magnitude of this peak. A calibration mixture of 0.9 ppmv of methane in nitrogen was investigated both before and after the ambient air sample. The PA signals at the peak wavelength agreed within 1% for the two calibrations. A comparison of the calibrated signal with the observed signal gives a methane concentration in air of 1.84 ± 0.02 ppmv. An alternative approach to obtaining the concentration is to simulate the measured spectrum by use of the HITRAN data base. The spectrum of the GIOPO output and the scaling of the PA signal can be obtained from the calibration run. By adjusting the methane concentration and the water-vapor concentration in the HITRAN program one can simulate the recorded spectrum by a convolution with the 0.8-cm^{-1}-broad Gaussian line shape of the GIOPO. The simulation was performed for a number of water and methane concentrations. A comparison of the experimental data for air (filled circles in Fig. 9) with the convoluted HITRAN spectrum of 0.45% water and 1.84 ppm of methane in an $80\%N_2/20\%O_2$ mixture at 291 K (solid curve in Fig. 9) shows that the agreement is very good at the 2948-cm^{-1} transition of methane, where water absorption shows little or no influence on the peak intensity of this transition. There appears to be an additional weak and broad structure at 2953–2961 cm^{-1}. This could be due to contributions to the PA signal by other hydrocarbon molecules in the air sample. The agreement of the two methods of analysis indicates that by setting the GIOPO at the peak of the 2948-cm^{-1} transition one can perform precise real-time monitoring of the methane concentration in ambient air on a continual long-term basis.

We accomplished similar *in situ* measurements at different times of day and on different days. The intraday variation of the methane concentration was ±0.03 ppmv, whereas the interday variation was as much as ±0.2 ppmv (~11%), to be compared with $a <$ 1% rms variations. In fact, the methane concentration can have large swings in a local metropolitan environment. Therefore the results are of interest for environmental protection research and for regional geophysical studies. A similar measurement in a rural setting will provide additional information.

4. Discussion

The measurements presented here are, to the best of our knowledge, the first calibration and concentration measurements of methane extended to the low-ppbv range. Because certified gas mixtures are not available in this concentration range, two methods can be applied, namely, diluting a certified gas mixture by adding nitrogen in a large container or in a flow system. In the first case methane would be dosed into the evacuated container through a needle valve until the required partial pressure were reached, and then the container would be filled with nitrogen to the ambient pressure. Because a part of the methane molecules may physisorb on the inner surface of the container, more methane molecules would be dosed into the container than needed for the required concentration in the gas phase. A portion of these adsorbed methane molecules would be replaced by nitrogen molecules during the filling process. Thus the methane concentration in the gas phase could increase in an uncontrolled way. This effect is more pronounced at small methane concentrations because the ratio of the adsorbed molecules to the molecules in the gas phase increases with decreasing concentration. Therefore this method is not suitable for purposes of accurate calibration.

The calibration gas in a flow system can be diluted with MFCs to produce extremely small concentrations.[28] However, the errors introduced by the MFCs may significantly influence the accuracy of the mixture concentration. The problem of the absolute error of the MFCs was discussed above. Our measurements indicate a smaller error than the guaranteed 1% of the full scale, because reproducible measurements could be carried at the lowest settings

of the MFCs. Nevertheless, the guaranteed 1% error must be used because no individual calibrations are available for the MFCs.

Another problem for calibration of the PA detector in a flow system is stability of the gas pressure. Because the PA signal is proportional to the number (mass) density of the absorbing molecules, the PA signal depends not only on the relative volume concentration (mixing rate) but also on the pressure. MFCs, while they maintain the adjusted flow, slightly modify the pressure. This effect results in fluctuations of the PA signal, even at constant volume flow. One can increase the accuracy of the calibration procedure by simultaneously monitoring the pressure and normalizing the measured PA signal to constant pressure.

In spite of these difficulties the calibration measurements performed reached an unprecedented accuracy. As is clearly demonstrated by these measurements, the usual calibration method of fitting a straight line to PA data measured at high and medium concentrations and extrapolating this line to the low-ppbv or even the parts in 10^{12} range may be fundamentally wrong. As can be seen from Fig. 4, the presence of the background signal modifies the value of the PA signal that is already at relatively high concentrations. A straight line fitted to the data points in the 100–1000-ppbv range possesses a substantially smaller slope than the true linear PA function shown as the dotted–dashed curve in Fig. 4. However, the vectorial fit function provides a perfect quantitative description of the measured PA signal also at small concentrations. Thus this method of signal analysis can be used for accurate PA trace-gas measurements. The parameters needed for calculating the concentration from the PA data with the fit function can be obtained by calibration of the system with certified gas mixtures and by background, noise, and phase measurements, as described.

5. Conclusions

The measurements of methane concentrations in ambient air by the GIOPO PA system have demonstrated the excellent performance of this device and the superiority of the method used for data analysis. Fluctuations of the methane concentration in ambient air were followed practically in real time with 1% accuracy. Because of the small sample volume and the fast time response of the GIOPO PA system, it could be used for monitoring fast local changes of ambient methane concentrations. The 1.2-ppbv sensitivity achieved in this experiment can be substantially improved by use of multiple passes in the resonant PA cell and by an increase in the output power of the GIOPO. Reducing the linewidth of the GIOPO to the order of 0.1 cm^{-1} will also improve the selectivity.

It is important to note that the GIOPO system is simpler than difference-frequency generation devices. For comparable laser power, the PA detector used has a sensitivity similar to that of a multipass absorption cell but a substantially smaller sample volume. Therefore the time needed for gas exchange during operation is much less (~10 s). Moreover, long-path absorption measures the difference between two large transmission signals with multiple reflections on mirror surfaces. The possibilities for errors in long-term continuous measurements as a result of stability problems or cell contamination are larger than in a single-pass PA measurement. Hence, even though the absorption scheme that uses single-mode laser diodes has the advantage of clearly better selectivity, the GIOPO PA scheme is an attractive alternative for fast and sensitive trace-gas analysis.

Financial support of this study by the bilateral scientific cooperation project between Germany and Taiwan (DAAD: D/9922931 and NSC 0890043921) is gratefully acknowledged. The Taiwan portion of this research is also partially supported by the China Petroleum Corporation.

References

1. C. R. Webster, R. D. May, C. A. Trimble, R. G. Chave, and J. Kendall, "Aircraft (ER-2) laser infrared absorption spectrometer (ALIAS) for *in-situ* stratospheric measurements of HCl, N_2O, CH_4, NO_2, and HNO_3," Appl. Opt. **33,** 454–472 (1994).
2. F. G. Wienhold, H. Fischer, P. Hoor, V. Wagner, R. Königstedt, G. W. Harris, J. Anders, R. Grisar, M. Knothe, W. J. Riedel, F.-J. Lübken, and T. Schilling, "TRISTAR—a tracer *in situ* TDLAS for atmospheric research," Appl. Phys. B **67,** 411–417 (1998).
3. D. Richter, D. G. Lancaster, and F. K. Tittel, "Development of an automated diode-laser-based multicomponent gas sensor," Appl. Opt. **39,** 4444–4450 (2000).
4. A. A. Kosterev, R. F. Curl, F. K. Tittel, C. Gmachl, F. Capasso, D. L. Sivco, J. N. Baillargeon, A. L. Hutchinson, and A. Y. Cho, "Effective utilization of quantum-cascade distributed-feedback lasers in absorption spectroscopy," Appl. Opt. **39,** 4425–4430 (2000).
5. D. G. Lancaster, R. Weidner, D. Richter, F. K. Tittel, and J. Limpert, "Compact CH_4 sensor based on difference frequency mixing of diode lasers in quasi-phasematched $LiNbO_3$," Opt. Commun. **176,** 461–468, (2000).
6. C. R. Webster, G. J. Flesch, D. C. Scott, J. E. Swanson, R. D. May, W. S. Woodward, C. Gmachl, F. Capasso, D. L. Sivco, J. M. Baillargeon, A. L. Hutchinson, and A. Y. Cho, "Quantum-cascade laser measurements of stratospheric methane and nitrous oxide," Appl. Opt. **40,** 321–326 (2001).
7. A. A. Kosterev, A. L. Malinovsky, F. K. Tittel, C. Gmachl, F. Capasso, D. L. Sivco, J. N. Baillargeon, A. L. Hutchinson, and A. Y. Cho, "Cavity ringdown spectroscopic detection of nitric oxide with a continuous-wave quantum-cascade laser," Appl. Opt. **40,** 5522–5529 (2001).
8. K. W. Busch and M. A. Busch, eds., *Cavity Ringdown Spectroscopy* (Oxford U. Press, New York, 1999).
9. L. B. Kreuzer, "Ultralow gas concentration infrared absorption spectroscopy," J. Appl. Phys. **42,** 2934–2943 (1971).
10. A. Miklós, P. Hess, and Z. Bozoki, "Application of acoustic resonators in photoacoustic trace gas analysis and metrology," Rev. Sci. Instrum. **72,** 1937–1955 (2001).
11. B. A. Paldus, T. G. Spence, R. N. Zare, J. Oomens, F. J. M. Harren, D. H. Parker, C. Gmachl, F. Capasso, D. L. Sivco, J. N. Baillargeon, A. L. Hutchinson, and A. Y. Cho, "Photoacoustic spectroscopy using quantum cascade lasers," Opt. Lett. **24,** 178–180 (1999).
12. K. Kuhnemann, K. Schneider, A. Hecker, A. A. E. Martis, W.

Urban, S. Schiller, and J. Mlynek, "Photoacoustic trace-gas detection using a cw single-frequency parametric oscillator," Appl. Phys. B **66,** 741–745 (1998).
13. D. Hofstetter, M. Beck, J. Faist, M. Nägele, and M. W. Sigrist, "Photoacoustic spectroscopy with quantum cascade distributed feedback lasers," Opt. Lett. **26,** 887–889 (2001).
14. S. Schaefer, M. Mashni, J. Sneider, A. Miklós, P. Hess, H. Pitz, K.-U. Pleban, and V. Ebert, "Sensitive detection of methane with a 1.65 μm diode laser by photoacoustic and absorption spectroscopy," Appl. Phys. B **66,** 511–516 (1998).
15. A. Bohren and M. W. Sigrist, "Optical parametric oscillator based difference frequency laser source for photoacoustic trace gas spectroscopy in the 3 μm mid-IR range," Infrared Phys. Technol. **38,** 423–435 (1997).
16. M. Seiter and M. W. Sigrist, "On-line multicomponent trace-gas analysis with a broadly tunable pulsed difference frequency laser spectrometer," Appl. Opt. **38,** 4691–4698 (1999).
17. C. Fischer, Q. Yu, M. Seiter, and M. W. Sigrist, "Photoacoustic monitoring of trace gases using a diode-based difference frequency laser source," Opt. Lett. **26,** 1609–1611 (2001).
18. C.-S. Yu and A. H. Kung, "Grazing-incidence periodically poled $LiNbO_3$ optical parametric oscillator," J. Opt. Soc. Am. B **16,** 2233–2238 (1999).
19. G.-C. Liang, H.-H. Liu, A. H. Kung, Á. Mohácsi, A. Miklós, and P. Hess, "Photoacoustic trace gas detection of methane using compact solid state lasers," J. Phys. Chem. A **104,** 10,179–10,183 (2000).
20. S. C. Tyler, H. O. Ajie, M. L. Gupta, R. J. Cicerone, D. R. Blake, and E. J. Dlugokencky, "Stable carbon isotopic composition of atmospheric methane: a comparison of surface level and free tropospheric air," J. Geophys. Res. **104,** 13,895–13,910 (1999).
21. D. A. Bossio, W. R. Horwath, R. G. Mutters, and C. van Kessel, "Methane pool and flux dynamics in a rice field following straw incorporation," Soil Biol. Biochem. **31,** 1313–1322 (1999).
22. S. P. Hesselbo, D. R. Gröcke, H. C. Jenkyns, C. J. Bjerrum, P. Farrimond, H. S. M. Bell, and O. R. Green, "Massive dissociation of gas hydrate during a Jurassic oceanic event," Nature **406,** 392–395 (2000).
23. R. L. Saaa, F. M. Fisher, Jr., A. Ding, and Y. Huang, "Exchange of methane from rice fields: national, regional, and global budgets," J. Geophys. Res. **104,** 26,943–26,951 (1999).
24. HITRAN Database. Last update, 21 September 2001. http://www.hitran.com.
25. A. Schmohl, A. Miklós, and P. Hess, "Effects of adsorption–desorption processes on the response time and accuracy of photoacoustic detection of ammonia," Appl. Opt. **40,** 2571–2578 (2001).
26. S. Schaefer, A. Miklós, and P. Hess, "Quantitative signal analysis in pulsed resonant photoacoustics," Appl. Opt. **36,** 3202–3211 (1997).
27. S. Schaefer, A. Miklós, A. Pusel, and P. Hess, "Absolute measurement of gas concentrations and saturation behavior in pulsed photoacoustics," Chem. Phys. Lett. **285,** 235–239 (1998).
28. M. Nägele and M. W. Sigrist, "Mobile laser spectrometer with novel resonant multipass photoacoustic cell for trace-gas sensing," Appl. Phys. B **70,** 985–901 (2000).